

University of Dundee

Sequence differences between BAX and BAK core domains manifest as differences in their interactions with lipids

Miller, Michelle S.; Cowan, Angus D.; Brouwer, Jason M.; Smyth, Sean T.; Peng, Liuyu; Wardak, Ahmad Z.

Published in:
FEBS Journal

DOI:
[10.1111/febs.17031](https://doi.org/10.1111/febs.17031)

Publication date:
2024

Licence:
CC BY

Document Version
Publisher's PDF, also known as Version of record

[Link to publication in Discovery Research Portal](#)

Citation for published version (APA):

Miller, M. S., Cowan, A. D., Brouwer, J. M., Smyth, S. T., Peng, L., Wardak, A. Z., Uren, R. T., Luo, C., Roy, M. J., Shah, S., Tan, Z., Reid, G. E., Colman, P. M., & Czabotar, P. E. (2024). Sequence differences between BAX and BAK core domains manifest as differences in their interactions with lipids. *FEBS Journal*, 291(11), 2335-2353. <https://doi.org/10.1111/febs.17031>





General rights

Copyright and moral rights for the publications made accessible in Discovery Research Portal are retained by the authors and/or other copyright owners and it is a condition of accessing publications that users recognise and abide by the legal requirements associated with these rights.

Take down policy

If you believe that this document breaches copyright please contact us providing details, and we will remove access to the work immediately and investigate your claim.

Sequence differences between BAX and BAK core domains manifest as differences in their interactions with lipids

Michelle S. Miller^{1,2} , Angus D. Cowan^{1,2}, Jason M. Brouwer^{1,2}, Sean T. Smyth¹, Liuyu Peng³, Ahmad Z. Wardak¹, Rachel T. Uren^{1,2}, Cindy Luo¹, Michael J. Roy^{1,2} , Sayali Shah^{1,2}, Ziwen Tan^{1,2}, Gavin E. Reid^{3,4,5}, Peter M. Colman^{1,2}  and Peter E. Czabotar^{1,2} 

1 Walter and Eliza Hall Institute of Medical Research, Parkville, Vic., Australia

2 Department of Medical Biology, University of Melbourne, Parkville, Vic., Australia

3 School of Chemistry, University of Melbourne, Parkville, Vic., Australia

4 Department of Biochemistry and Pharmacology, University of Melbourne, Parkville, Vic., Australia

5 Bio21 Molecular Science and Biotechnology Institute, University of Melbourne, Parkville, Vic., Australia

Keywords

apoptosis; BAK; BAX; BCL2; lipid binding

Correspondence

M. S. Miller, P. M. Colman and

P. E. Czabotar, Walter and Eliza Hall

Institute of Medical Research, 1G Royal

Parade, Parkville, Vic., Australia

Tel: +61 3 9345 2555

E-mail: miller.m@wehi.edu.au; pcolman@wehi.edu.au

czabotar@wehi.edu.au

Michelle S. Miller and Angus D. Cowan

contributed equally to this article

(Received 18 September 2023, revised 7 November 2023, accepted 11 December 2023)

doi:10.1111/febs.17031

The B-cell lymphoma 2 (BCL2) family members, BCL2-associated protein X (BAX) and BCL2 homologous antagonist killer (BAK), are required for programmed cell death via the mitochondrial pathway. When cells are stressed, damaged or redundant, the balance of power between the BCL2 family of proteins shifts towards BAX and BAK, allowing their transition from an inactive, monomeric state to a membrane-active oligomeric form that releases cytochrome *c* from the mitochondrial intermembrane space. That oligomeric state has an essential intermediate, a symmetric homodimer of BAX or BAK. Here we describe crystal structures of dimers of the core domain of BAX, comprising its helices $\alpha 2$ – $\alpha 5$. These structures provide an atomic resolution description of the interactions that drive BAX homo-dimerisation and insights into potential interaction between core domain dimers and membrane lipids. The previously identified BAK lipid-interacting sites are not conserved with BAX and are likely to determine the differences between them in their interactions with lipids. We also describe structures of heterodimers of BAK/BAX core domains, yielding further insight into the differences in lipid binding between BAX and BAK.

Introduction

The intrinsic (or mitochondrial) cell-death pathway is controlled by the BCL2 family of proteins, some members of which promote cell death whilst others restrain it. The family is aroused via interactions with small proteins possessing only the third sequence homology motif, known as the BH3-only proteins, that are sensors of cellular stress or redundancy. Interactions between BH3-only proteins and pro-survival family

members are long-lived whilst those with pro-apoptotic BAX/BAK are transient and trigger conformational re-arrangements in BAX/BAK that lead to their oligomerisation and consequent permeabilisation of the mitochondrial outer membrane [1].

The BCL2 protein family fold is a bundle of eight α -helices characterised by four motifs of sequence similarity designated BH1 through BH4 [2]. A ninth helix

Abbreviations

BAK, BCL2 homologous antagonist killer; BAX, BCL2 associated protein X; BCL2, B-cell lymphoma 2; CL, cardiolipin; diC8-PS, di-octanoyl phosphatidylserine; GFP, Green Fluorescent Protein; lysoPC, 2-stearoyl-*sn*-glycero-3-phosphocholine; MLM, mouse liver mitochondria; PE, phosphatidylethanolamine; PEG, polyethylene glycol; PG, phosphatidylglycerol; TLC, thin layer chromatography; WT, wild-type.

facilitates association with or anchoring in the mitochondrial outer membrane. This fold is a feature of both the pro-survival BCL2 family members (BCL2 itself, BCLXL, BCLW, MCL1 and BFL1 [3]) and pro-apoptotic members (BAX [4,5] and BAK [6]). The BH3 sequence motif is located within helix $\alpha 2$. A groove on the surface of the BCL2 fold delineated by helices $\alpha 3$, $\alpha 4$ and $\alpha 5$ forms a receptor site for the helical BH3 motif of BH3-only proteins, such as BIM or BID.

Upon engaging BIM or BID, both BAX and BAK separate into core ($\alpha 2$ – $\alpha 5$) and latch ($\alpha 6$ – $\alpha 8$) domains [7,8], with $\alpha 1$ dissociated from both [9]. Detergents are also able to activate BAX [7,10], although some zwitterionic detergents have been reported to inhibit BAX [11]. Once freed from the BCL2 fold upon activation, core domains of BAX or BAK homodimerise by insertion of $\alpha 2$ from one polypeptide into the $\alpha 3\alpha 4\alpha 5$ groove of the other protomer [12]. These core domain dimers are amphipathic, and we have proposed that their lipophilic face, comprising a platform of helices $\alpha 4\alpha 5$ – $\alpha 5'\alpha 4'$, initially associates with the mitochondrial membrane in the manner of a monotopic membrane protein [7]. Subsequent oligomerisation of these dimers correlates with release of factors from the mitochondrial intermembrane space [13]. Various models are contemplated for the organisation of multimers of core dimers within the membrane pore [14,15].

Crystals of the BAX core domain fused to Green Fluorescent Protein (GFP) provided the first image of core domain dimers [7], albeit at a resolution sufficient

only to confirm the helical fold but not to unambiguously locate side chains (PDB: 4BDU). Another picture was provided by an NMR structure of the BAX core dimer in the context of a lipid bicelle (PDB: 6L8V) [16], which despite a similar helical arrangement, displays significant differences when compared with the crystal structure. High-resolution crystal structures of BAK core dimers [8], including in complex with lipids and detergents [17], have been published. In the latter case, amino acids implicated in BAK binding to lipids are not strictly conserved in BAX (Fig. 1), raising questions about the generality of core dimer interactions with lipids.

Here we describe high-resolution crystal structures of BAX core domain dimers, both in the absence and presence of lipids. In contrast to previous structures of BAK core dimers with lipid [17], for BAX we were unable to identify electron density that unambiguously represented lipid molecules. However, the molecular dyad symmetry of the dimers is disturbed in the crystal structures that contain lipids, implicating residues involved in lipid interactions.

Results

BAX $\alpha 2$ – $\alpha 5$ (residues D53–K128, with the mutations C62S and C126S) was expressed and purified as an N-terminally fused GST-tagged protein. Subsequent purification following cleavage of the GST-tag yielded two distinct species: a tetramer fraction and a hexamer fraction, approximately 40 and 63 kDa in size,

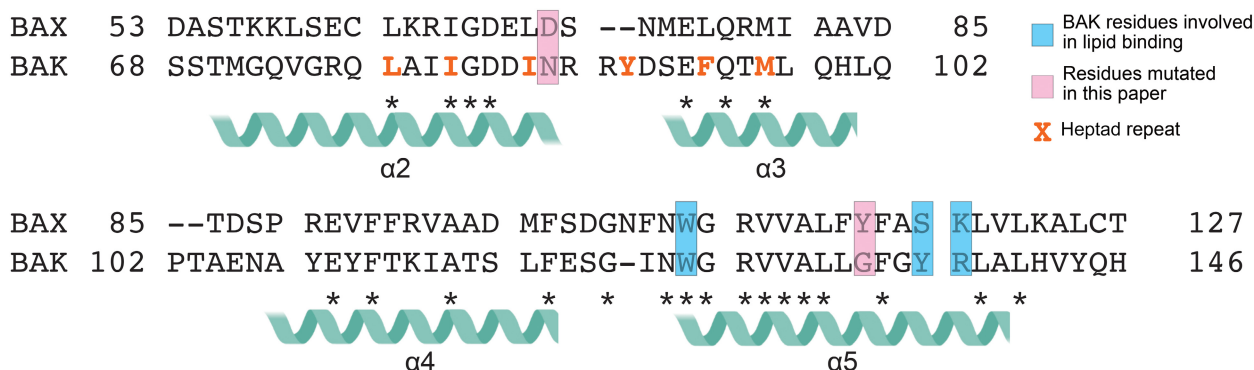


Fig. 1. Structural alignment of *hsBAX* and *hsBAK* throughout their core domains. Sequence alignment of BAX (Q07812) $\alpha 2$ – $\alpha 5$ with BAK (Q16611) $\alpha 2$ – $\alpha 5$ based on a structural superposition generated with PYMOL. BAK residue W125 is the only lipid interacting amino acid conserved in BAX (W107 – lipid interacting residues identified in [17] are highlighted in blue). Notable differences between the sequences are highlighted in pink and include BAX residues D71 (N86 in BAK) and Y115 (G133 in BAK). The amino acids in BAK helices $\alpha 2$ and $\alpha 3$ (orange letters) suggest a (near) continuous heptad repeat of hydrophobic residues through the $\alpha 2$ – $\alpha 3$ linker that is disrupted by the deletion in BAX. Sequence alignment might prefer the BAX deletion at BAK residues D90–S91, but the structural alignment is indicated here. BAK Y89 can be considered as a fifth hydrophobic residue ('h5') of its BH3 motif, being buried in the structure of the core dimer (PDB: 6UXM) in which helices $\alpha 2$ and $\alpha 3$ are continuous with a kink.

respectively (elution volume 11.3 and 10.4 mL, respectively) (Fig. S1). All of the new structures we describe here for this BAX core domain construct display as homodimers, never monomers, consistent with earlier studies of both BAX [7] and BAK [8,17]. Both the tetramer and hexamer fractions crystallised under multiple conditions, yielding different crystal forms with complementary views of the dimer.

BAX tetramer fraction crystals reveal key structural difference between BAK and BAX dimers

Type 1 and 2 crystals (tetramer)

In this crystal form of the BAX tetramer, four dimers in the asymmetric unit are arranged in two D2-symmetric tetramers (Type 1 in crystals, Table 1, Fig. 2A). The arrangement of helices in the dimer

structure does not differ from that described previously in a fusion protein with GFP (PDB: 4BDU, BAX dimer regions estimated resolution $\sim 4 \text{ \AA}$ [7]), though here it is observed at high resolution (2.1 \AA), enabling scrutiny of sidechain interactions. Minor differences between the four dimer structures are observed at the termini of the construct, the $\alpha 3$ - $\alpha 4$ corner and at F114 which adopts different rotamers to accommodate its symmetry partners in the D2 particle (Fig. S2).

In terms of dimer topology, helix $\alpha 2$ from one polypeptide inserts into the $\alpha 3\alpha 4\alpha 5$ groove of its partner in the dimer (Fig. 2A). The dimer structure is characterised by two extended $\alpha 2\alpha 3$ segments and two hairpin $\alpha 4\alpha 5$ segments in a two-layered structure around a hydrophobic core. The former layer presents a hydrophilic exterior and the latter a hydrophobic one. We have previously proposed for BAX [7] and BAK [8] that, following separation of the core and latch

Table 1. Crystallographic data table for BAX core dimer structures. Statistics for the highest-resolution shell are shown in parentheses.

	Type 1. Tetramer 8G1T	Type 2. Tetramer 8SPE	Type 3. Hexamer with 2-stearoyl lysoPC 8SPF	Type 4. Hexamer with diC8-PS 8SPZ	BAX D71N hexamer 8SVK
Space group	P2 ₁	P3 ₁	P2 ₁ 2 ₁ 2 ₁	P2 ₁ 2 ₁ 2	P3 ₁ 21
Unit cell					
<i>a</i> , <i>b</i> , <i>c</i> (Å)	60.36, 70.37, 62.78	141.34, 141.34, 110.18	61.13, 83.88, 100.3	52.81, 88.07, 73.30	67.39, 67.39, 140.82
α , β , γ (°)	90, 90.14, 90	90, 90, 120	90, 90, 90	90, 90, 90	90, 90, 120
Wavelength (Å)	0.9537	0.9537	0.9537	0.9537	0.9537
Resolution range (Å)	50.0–2.09 (2.16–2.09)	50.0–2.30 (2.44–2.30)	50.0–2.20 (2.33–2.20)	50.0–2.40 (2.49–2.40)	36.58–2.25 (2.33–2.25)
Total reflections	112 743 (10 290)	622 201 (99 217)	167 737 (18 128)	61 008 (6225)	181 955 (18 467)
Unique reflections	30 871 (2935)	108 455 (17 395)	26 715 (4056)	13 894 (1352)	18 217 (1775)
Multiplicity	3.7 (3.5)	5.7 (5.7)	6.3 (4.5)	4.4 (4.6)	10.0 (10.4)
Completeness (%)	98.9 (93.4)	99.8 (98.9)	99.1 (94.5)	99.7 (100)	99.9 (99.8)
<i>I</i> / σ (<i>I</i>)	9.1 (1.1)	11.71 (1.35)	15.8 (0.60)	16.7 (1.1)	11.43 (0.76)
<i>R</i> _{merge}	0.102 (1.81)	0.108 (1.56)	0.051 (2.01)	0.051 (1.39)	0.155 (3.04)
CC 1/2	0.997 (0.33)	0.998 (0.530)	1.00 (0.30)	1.00 (0.395)	0.99 (0.302)
<i>R</i> -work	0.2071 (0.3672)	0.2286 (0.3179)	0.2497 (0.3700)	0.2671 (0.3501)	0.2539 (0.3431)
<i>R</i> -free	0.2469 (0.3721)	0.2539 (0.3350)	0.3012 (0.3665)	0.3398 (0.3506)	0.2872 (0.3683)
Number of non-hydrogen atoms	4513	18 988	3285	2244	2410
Macromolecules	4454	18 910	3211	2229	2321
Ligands	4	40	59	15	69
Solvent	55	38	15	10	20
RMS					
Bonds (Å)	0.009	0.013	0.003	0.009	0.002
Angles (°)	1.25	0.98	0.81	1.22	0.46
Ramachandran					
Favoured (%)	94.17	94.67	95.04	93.36	95.44
Outliers (%)	0.18	0.94	0.25	1.11	0.70
Average B-factor					
Macromolecules	59.89	66.39	96.55	76.59	70.62
Ligands	61.69	59.46	98.36	103.5	78.47
Solvent	58.38	55.06	80.87	73.01	56.30

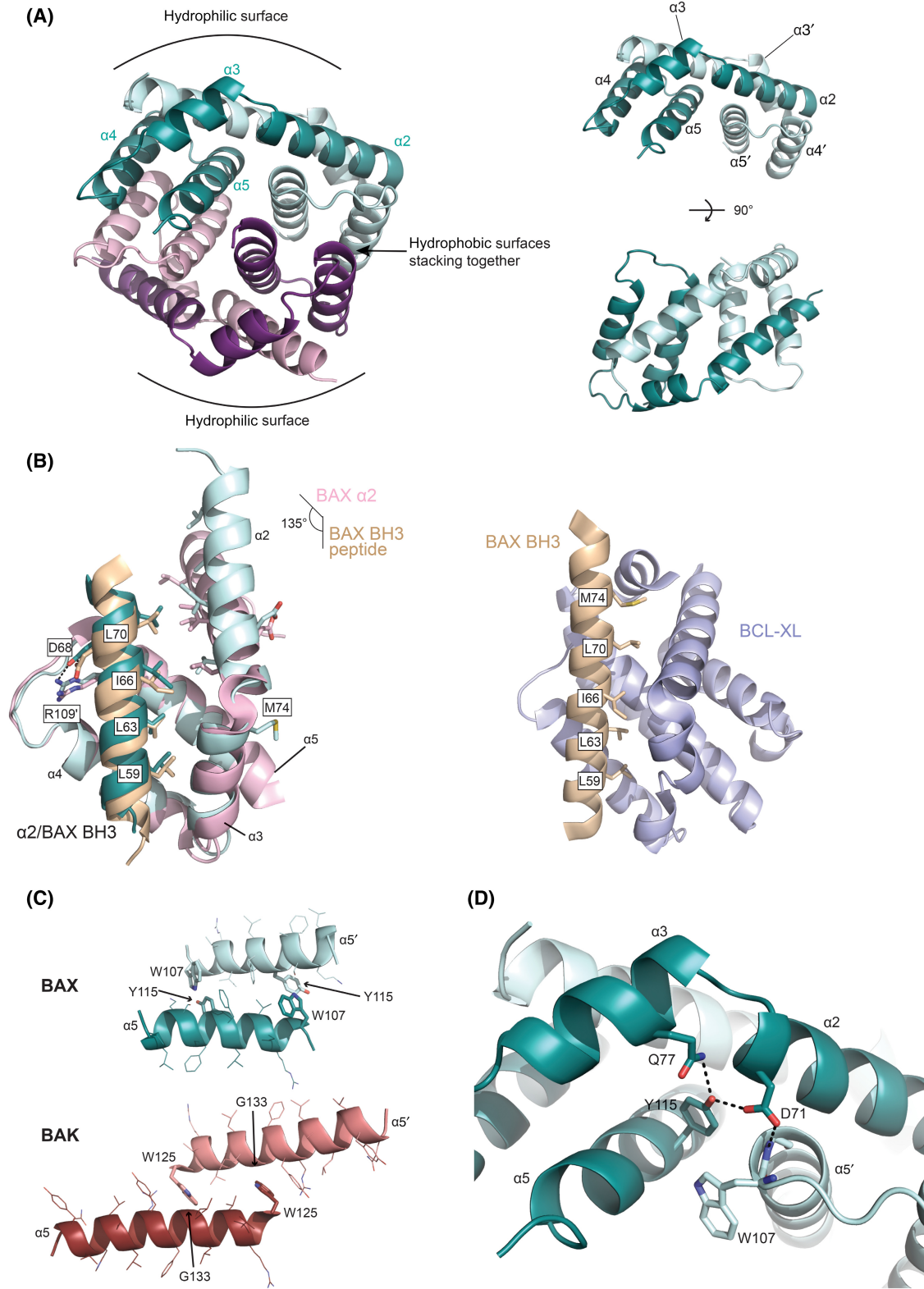


Fig. 2. BAX core dimers from the tetramer fraction. (A) Orthogonal views of BAX core dimers in Type 1 crystals. The left figure shows the arrangement of the dimers as a D2 tetrameric particle: dimer 1 is shown as dark (chain A) and light (chain B) teal, while dimer 2 is shown as purple (chain C) and light pink (chain D). Helices $\alpha 2$ – $\alpha 5$ are labelled. The upper right view shows the twisted hydrophobic platform $\alpha 4\alpha 5$ – $\alpha 5'\alpha 4'$ of dimer 1, while the lower right view shows the view into the hydrophilic surface formed by the pair of anti-parallel $\alpha 2\alpha 3$ helices. (B) Left: BAX core dimer interactions illustrating on the dark teal chain the four signature hydrophobic residues of the BH3 motif, L59, L63, I66 and L70 and the salt bridge D68–R109'. Note, as illustrated on the light teal chain, M74, involved in interactions with pro-survival proteins [19], is not engaged in core dimer formation. These contacts mimic those seen in the complex between the BAX BH3 peptide (wheat) and BAX (pink, PDB: 4BD6) in the upper layer where I66, L70, I66' and L70' cluster around the dyad axis (no electron density observed for M74). Right: BAX BH3 peptide bound to pro-survival BCL-XL (PDB: 3PL7). In this case M74 acts as a fifth hydrophobic residue in the BH3 motif. (C) Comparison of the exposed hydrophobic surface of the $\alpha 5\alpha 5'$ interactions in core dimers of BAX (top, dark and light teal, residues N106 to L122) and BAK (bottom, dark and light red, N125 to H145, PDB: 6UXM [17]). BAX residue W107 is exposed on the surface whereas BAK residue W125 is buried in the interior, adjacent to G133'. BAX residue Y115, the structural equivalent of BAK G133, impedes W107 from adopting the rotamer of BAK W125. (D) Hydrogen-bonding interactions between Y115 ($\alpha 5$), D71 ($\alpha 2$) and Q77 ($\alpha 3$) in the BAX core dimer. D71 is also H-bonded to the backbone amide of G108' ($\alpha 5'$). While Y115 makes similar contacts in the structure of inert, monomeric BAX (in human, mouse and catfish), D71 forms an additional salt-bridge to R34 ($\alpha 1$).

domains triggered by engaging BH3 motifs, the hydrophobic surface of the $\alpha 4\alpha 5$ – $\alpha 5'\alpha 4'$ layer directly engages the cytosolic leaflet of the mitochondrial membrane in the manner of a monotopic membrane protein. Here that surface is closely packed against a symmetry partner in the D2 tetramer. No solvent or ligand molecules are observed at this dimer-dimer interface, in contrast to similar D2 particles of BAK core dimers [17]. Note, however, that the D2 particles of BAK were only ever observed by solubilising a D3-symmetric particle with detergents or lipids prior to crystallisation.

The hydrophobic core of each dimer contains the signature BAX BH3 ($\alpha 2$) hydrophobic residues L59, L63, I66 and L70 interacting with canonical groove receptor residues on helices $\alpha 3'$ (L76, M79, I80), $\alpha 4'$ (V91, V95, M99) and $\alpha 5'$ (F116) (Fig. 2B). Within all four dimers in the asymmetric unit the salt bridge between D68 ($\alpha 2$) and R109' ($\alpha 5'$) is observed. We extracted from the core dimers entities containing BH3-in-groove moieties, that is to say an $\alpha 2$ (the BH3 motif) from one polypeptide in the $\alpha 3\alpha 4\alpha 5$ groove of its partner, for the purpose of comparing this interaction with our previously published structure of a BAX BH3 peptide bound to BAX [7] (PDB: 4BD6, Fig. 2B). In the peptide bound structure, the angle between the BH3 peptide and $\alpha 2$ BH3 of BAX is approximately 135°, whereas in the core dimer structures the two $\alpha 2$ BH3s are approximately anti-parallel. Otherwise, no significant differences are observed. Residues I66, L70 and their partners (I66', L70') are close to the dyad symmetry axis of the core dimer and they are similarly close in the BAX:BAXBH3 peptide structure. This is consistent with all structures of BH3 peptides (whether of BAX, BID [7], or BIM [18]) bound to BAX, in the sense that the h3 and h4 residues of the peptide are juxtaposed to L70 (h4) and I66 (h3) of BAX, respectively.

M74 is a critical residue in facilitating restraint of BAX by pro-survival proteins yet M74 mutants pose no barrier to apoptosis [19]. M74 can be considered a fifth hydrophobic residue in the BH3 motif of BAX, as evidenced by its role in engaging the pro-survival proteins BCL-XL and MCL1 [19] (PDB: 3PL7 and PDB: 3PK1) and BCL2 [20] (PDB: 2XAO). In contrast, BAX core dimers form with M74 exposed to solvent and thus it does not contribute to BAX-BAX BH3:groove interaction, providing a rationale for why M74 mutations do not affect membrane permeabilisation (Fig. 2B).

A distinguishing feature in comparison to BAK core dimers is the location of the conserved tryptophan residue at the N-terminus of $\alpha 5$. BAX W107, and its symmetry counterpart, project outwards from the hydrophobic $\alpha 4\alpha 5$ – $\alpha 5'\alpha 4'$ surface of the dimer and are engaged in the interface between pairs of core dimers that constitute the D2 particle described above. In contrast, BAK W125 is buried within the interior of the BAK core dimers, packed against G133'. BAX residue Y115 (see Fig. 1) is likely responsible for this difference as it occupies the space where W107 might otherwise locate (Fig. 2C).

As noted above, BAX Y115 occludes entry of W107' into the interior of the core dimer structure. Y115 engages D71 and Q77 in hydrogen bonds, a similar environment to that observed in inert, monomeric BAX from mammals (PDB: 5W60, PDB: 5W61, PDB: 5W62) and catfish (PDB: 5W63) [4]. In those structures, D71 is close to R34 from $\alpha 1$, whereas in the core dimer D71 is also H-bonded to the backbone amide of G108' (Fig. 2D). On seven of the eight polypeptides in the asymmetric unit a water molecule is observed at the backbone amide of W107 and on the eighth a crystal contact intervenes. Thus the environment at the N-terminus of helix $\alpha 5$ is quite different to that observed in BAK core dimers [17] where N86 (Fig. 1)

is positioned over the backbone amide of G126' and an anion (e.g. the phosphate of a lipid head group) is bound to the backbone amide of W125'.

A second tetramer crystal form (type 2 in crystals, Table 1), containing 18 dimers in the asymmetric unit, had essentially the same dimeric topologies as in type 1 crystals, although some outliers within the asymmetric unit displayed disorder in the $\alpha 3$ and $\alpha 3$ - $\alpha 4$ linker, indicating softness in the structure in that region (Fig. S3).

Co-crystals of the BAX hexamer fraction with lipids reveal an asymmetric dimer

Type 3 crystals (hexamer with lysoPC)

Co-crystallising the hexamer in the presence of lipids yielded two distinct crystal forms, each of which displays some asymmetry in the dimer and distinct conformations from the tetramer crystals. The first (type 3) grew in the presence of 5 mM 2-stearoyl-*sn*-glycero-3-phosphocholine (lysoPC). The hexamer has pseudo-D3 symmetry with the hydrophilic surfaces of the dimers on the exterior of the D3 particle, somewhat reminiscent of a trimeric association of BAK core dimers [17] (Fig. 3A). Overlay of the six polypeptides reveals that the chains in the dimers C:D: and E:F: are indistinguishable from each other and from the conformation of the polypeptides in type 1 crystals (Fig. 3B). Chain A: is an outlier at W107 and the preceding $\alpha 4$ - $\alpha 5$ corner, and chain B: differs from the canonical fold in the pitch of $\alpha 2$ and its connections to $\alpha 3$, commencing at B:R65 and extending through B:'s disordered $\alpha 3$ (Fig. 3B). Thus, the A:B: dimer is inherently asymmetric.

Overlay of the three dimers shows that the anomalies in the conformation of chains A: and B: are correlated (Fig. 3C). In the canonical, type 1 symmetric dimers the side chains of W107 are exposed on the hydrophobic surface of the $\alpha 4\alpha 5$ - $\alpha 5'\alpha 4'$ layer of the dimer. Chain B:W107 adopts the canonical rotamer and A: $\alpha 2$ - $\alpha 3$ is similar to the polypeptides

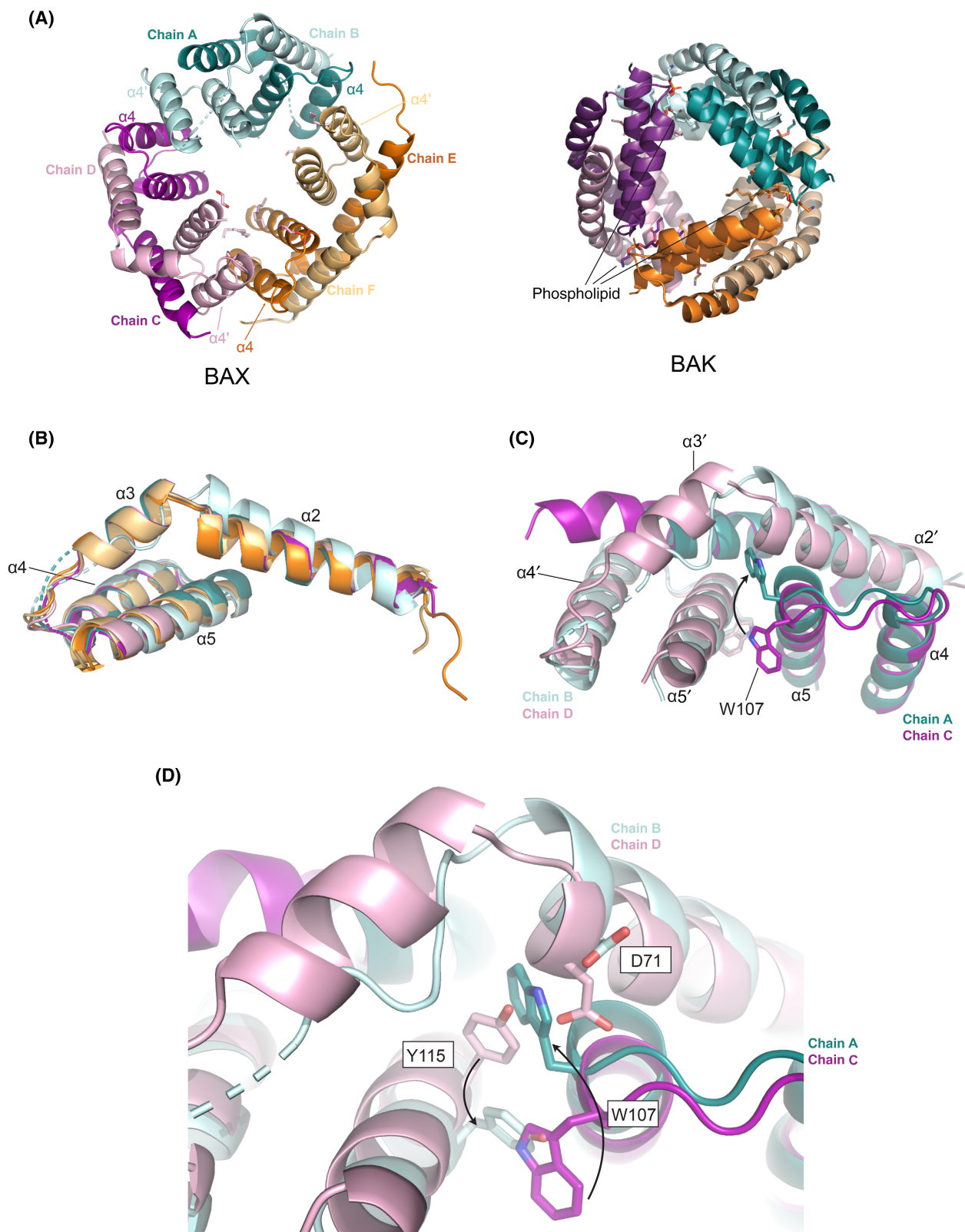
in the type 1 symmetric dimers. In contrast A:W107 is buried between the two layers of the A:B: dimer close to the $\alpha 2$ - $\alpha 3$ connection of chain B:, a feature reminiscent of BAK core dimers bound to lipid as described above. Chains A: and B: have elevated temperature factors compared to the others and within the A:B: dimer the poorest defined helices are B: $\alpha 3$, A: $\alpha 2$ and B: $\alpha 5$. Despite this, ensemble refinement [21], which yields a slightly improved Rfree (0.296), does not sample canonical rotamers for A:W107, confirming a distinct rotamer.

The asymmetry in the A:B: dimer stems from structural features in its hydrophobic platform ($\alpha 4\alpha 5$ - $\alpha 5'\alpha 4'$), notably the different rotamers of the two W107 residues. In order to accommodate the anomalous A:W107, B: $\alpha 5$ (and especially B:Y115) is dislocated (Fig. 3D). Whereas the canonical A:Y115 is buried in the core dimer interior (hydrogen bonded to A:D71 and A:Q77 as in type 1 crystals and inert, monomeric BAX), B:Y115 is remote from B:D71 and exposes its hydroxyl to the surface of the hydrophobic platform. We suggest that the lipidic interior of the D3 particle has influenced this outcome, but the crystal structure discloses no ligands associated with B:Y115.

Another way to compare the structural motifs in the core dimers is by alignment of the six BH3-in-groove entities, that is $\alpha 2$ (residues 60–71) of one chain with $\alpha 3\alpha 4\alpha 5$ (residues 72–128) of its partner in the dimer. Such alignments illustrate that, notwithstanding the disordered B: $\alpha 3$, no significant difference is observed (beyond the aforementioned side chains of C:W107 and D:Y115) (Fig. S4).

The three interfaces between the dimers in the D3 particle involve pairs of $\alpha 4$ helices, with F93 on one dimer close to F100 and F105 on the neighbour (Fig. S5). The interface between chains B: and C:, whilst still utilising these same aromatic residues, differs in atomic detail to the other two. The trimeric assembly of dimers through $\alpha 4$ contacts is like that observed in the molecular replacement solutions to the crystal structures that could not be successfully refined

Fig. 3. Co-crystals of the hexamer fraction with lipids reveal an asymmetric dimer. (A) Trimers of dimers in Type 3 crystals assemble with pseudo-D3 symmetry via tenuous contacts between $\alpha 4$ helices (left). No ordered lipids are observed. BAK core dimers form a particle of similar size (right, PDB: 6UXM [17]), with a lipid head group associated at the N-terminus of all $\alpha 5$ s, its proximal alkyl groups crosslinking adjacent dimers in the trimer and the distal alkyl groups disordered in the interior of the particle. (B) Overlay of six polypeptides in the D3 assembly of type 3 crystals. Chain B: (light teal) is an outlier, most clearly in the pitch of $\alpha 2$. (C) Overlay of the A:B: (dark/light teal) dimer with the C:D: (dark purple/light pink) dimer. The C:D: and E:F: dimers in Type 3 crystals are symmetric and identical to those of Type 1 crystals, but the A:B: dimer is asymmetric with anomalies at A:W107 and the pitch of B: $\alpha 2$. A:W107 is inserted between the two-layers of the core dimer, dislocating the B: $\alpha 2$ - $\alpha 3$ linker. (D) Environment of Y115 in symmetric core dimers (light pink & purple) compared to that of B: Y115 (light teal) where A:W107 (dark teal) is inserted between B:Y115 and B:D71 (light teal). Note that at the other end of the A:B: dimer, A:Y115 and B:W107 appear as in the pink/purple dimer.



(see [Materials and methods](#)). Buried surface areas for these three $\alpha 4$ - $\alpha 4$ interfaces are all smaller than 200 \AA^2 . This small contact surface is typical of contacts observed between protein molecules in a crystal lattice, not between proteins in an oligomeric assembly, suggesting that lipids drive the trimer assembly as proposed for BAK [17]. Indeed, bacterial lipids were purified along with the hexameric BAX core fraction (Fig. S6), as with BAK previously, but not the tetrameric fraction [17].

Although the protein used in preparing the type 3 crystals was incubated with lysoPC, whether any exchange occurred with endogenous lipids is not known. No electron density is observed either for bacterial lipids or for lysoPC. Fragments of electron density not belonging to protein have been variously modelled as ethylene glycol (from the crystal freeze), one glycerol-1-phosphate, and one each of an 8-, a 9- and a 12-carbon alkyl chain. These alkyl chains are associated with the exposed $\alpha 4\alpha 5$ surface of chain E: and at the $\alpha 4$ - $\alpha 4$ interface between chains A: and F:. The glycerol-1-phosphate moiety is at the N-terminus of E: $\alpha 5$.

Type 4 crystals (hexamer with di-octanoyl phosphatidylserine)

These crystals were grown in the presence of the short chain di-acyl lipid, di-octanoyl phosphatidylserine (diC8-PS). Under these conditions, the hexamer is disassembled, and core dimers appear in an extended helical array as described below (Fig. 4A). Two dimers constitute the crystallographic asymmetric unit, one (A:B:) being asymmetric (like A:B: in the type 3 crystals) and the other (C:D:) being a canonical symmetric dimer. Here chain A: has the anomalous W107 rotamer inserting the indole ring into the interior of the A: B: dimer, and chain B: has the anomalous pitch of $\alpha 2$ (Fig. 4B). Two sulfate ions from the crystallisation condition are observed at the backbone amides of W107 on chains B: and C:. Near the anomalous A: W107 a third sulfate is modelled but not over the N-terminus of A: $\alpha 5$. Rather, it is located 3.5 \AA from the exposed B:Y115 and B:K119. Small ($3\text{-}4\sigma$) difference electron density peaks adjacent to this sulfate ion are not inconsistent with the features of a poorly ordered lipid head group (Fig. S7).

The interface between B: $\alpha 4$ and D: $\alpha 4$ is similar to that seen between $\alpha 4$ helices in the D3 particle described above, but with an even smaller contact area. This contact is recapitulated between chain A: and chain C: of a symmetry-related dimer, resulting in a continuous helical structure throughout the crystal in

which the hydrophobic surfaces of the dimers face the helix axis, the crystal c-axis. The dyad axis along this cell edge generates a double helical assembly where A: B: dimers and C:D: dimers each face off their symmetry partners across a cavity along and around the helix axis (Fig. 4A). These cavities are continuous with each other and with neighbouring tetramers along the crystallographic dyad symmetry axis. It is likely that this cavity contains disordered lipid molecules. The resulting assembly is a double helical structure, with dimer contacting dimer through the exposed edges of $\alpha 4$ along the helix axis. Tenuous protein contacts across the helix axis involve residues at the C-terminus of the construct and bury only small surface areas ($\sim 100 \text{ \AA}^2$) on each polypeptide, typical of contacts in a crystal lattice as discussed for type 3 crystals.

BAX/BAK core domain heterodimer

A minor population of BAX/BAK heterodimers has previously been identified in cells [22]. Taking advantage of the proximity of the C-terminus of $\alpha 5$ to the N-terminus $\alpha 2$ in the homo-core dimers of BAK and BAX, we constructed a BAK core domain (S68-H145) linked to a BAX core domain (D53-K128) via the linker sequence (GGG)₄G. Given the differences in lipid binding between BAX and BAK that we have identified, we crystallised the hybrid core domains in the presence of the detergent C12E8 [12] and the lipid lysoPC to see if we could glean further insight into the BAX residues involved in lipid binding.

Type A crystals C12E8 crystals

These crystals grow in the presence of the detergent, C12E8. The asymmetric unit contains two fusion polypeptides, i.e. two hetero-core dimers assembled as heterodimers with the $\alpha 2$ from the BAK component in the $\alpha 3\alpha 4\alpha 5$ groove of the BAX component and vice versa (Fig. 5A). The structure of each polypeptide resembles the core domain dimer of BAK or BAX. The two hetero-core dimers are arranged in a pseudo-D2 symmetric particle, with BAK $\alpha 4\alpha 5$ facing off BAK $\alpha 4\alpha 5$; and BAX $\alpha 4\alpha 5$ facing off BAX $\alpha 4\alpha 5$.

Two essential differences to the homodimers arise. The heterodimer BH3-in-groove interactions involve the BAK $\alpha 2$ in the BAX $\alpha 3\alpha 4\alpha 5$ groove and of BAX $\alpha 2$ in the BAK $\alpha 3\alpha 4\alpha 5$ groove (Fig. 5B, Fig. S8), and the centre of the lipophilic $\alpha 4\alpha 5$ - $\alpha 5'$ - $\alpha 4'$ platform accommodates $\alpha 5$ sequence differences between BAK and BAX. Unlike in BAK homodimers, both BAK W125 residues on both heterodimers in the tetrameric particle are exposed in the $\alpha 4\alpha 5$ - $\alpha 5'$ - $\alpha 4'$ surface

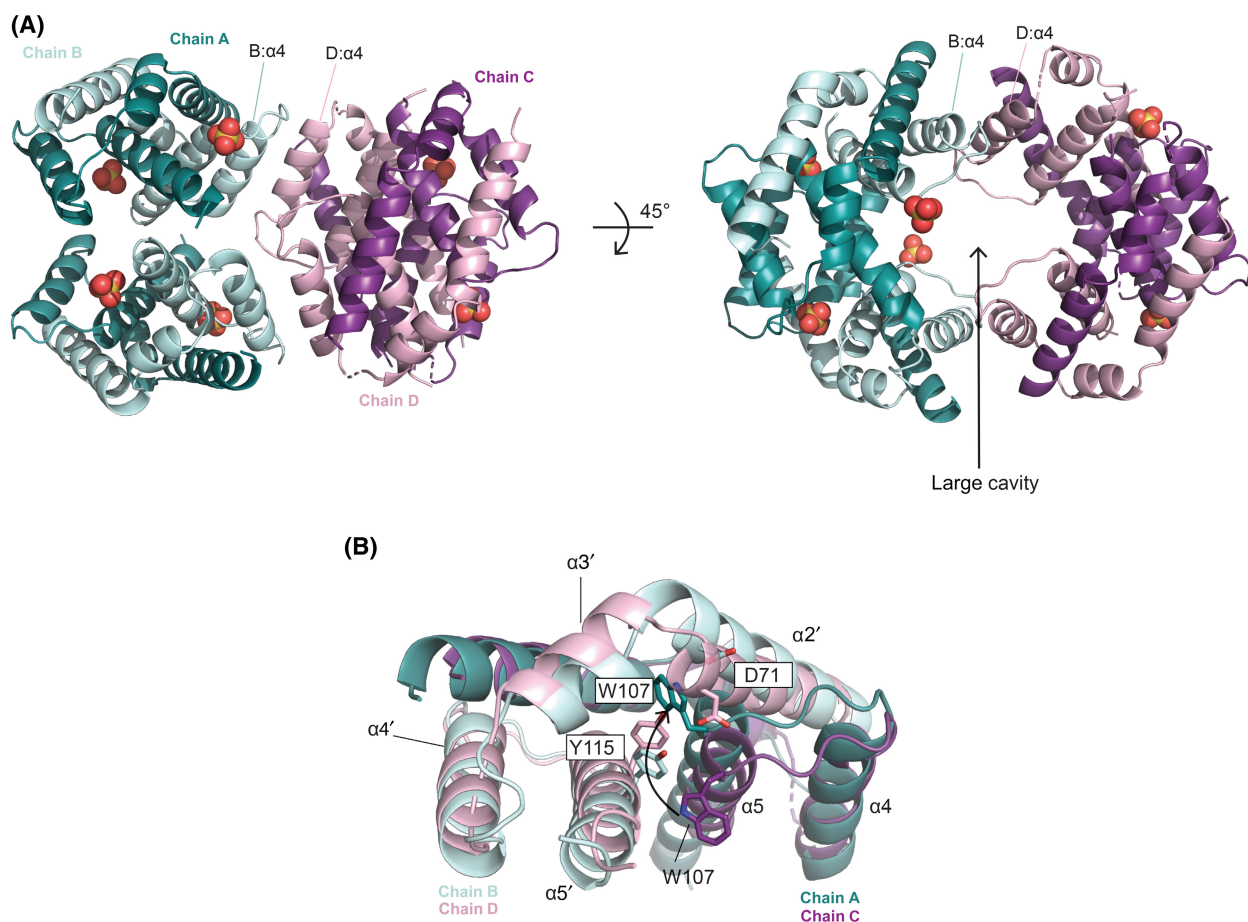


Fig. 4. Co-crystals of the hexamer fraction with di-octanoyl phosphatidylserine form a helical arrangement with a mixture of symmetric and asymmetric dimers. (A) Assembly of asymmetric (A:dark teal, B:light teal) and symmetric (C:purple, D:light pink) dimers around the crystallographic dyad axis (horizontal in both images). Unlike the closely packed tetramers of crystal Types 1 and 2, here the association is around a cavity along the dyad axis which is presumed to contain the short-chain lipid, di-octanoyl phosphatidylserine. The modelled sulfate ions (depicted as yellow and red spheres) could instead be poorly-ordered head groups of these lipids. The A:B and C:D dimers contact each other via B: $\alpha 4$ and D: $\alpha 4$. The motif shown extends through the crystal along the dyad axis via similar contacts between A: $\alpha 4$ (dark teal) and C: $\alpha 4$ (purple). (B) Overlay of the asymmetric (A: dark teal, B: light teal) and symmetric (C: purple, D: light pink) dimers showing the anomalous pitch of $\alpha 2'$ and insertion of A:W107.

because the adjacent BAX residue Y115 prevents its insertion into the interior of the dimer. BAX W107, although adjacent to BAK G133, does not insert either (Fig. 5C) (as observed in both chains of symmetric BAX dimers and one chain of asymmetric BAX dimers). This is unanticipated as BAK homodimer structures have a cavity at this location due to the smaller sidechain of BAK G133. Instead, in this heterodimer structure, density from the crystallisation condition is present in the cavity and has been modelled as fragments of polyethylene glycol (PEG) and C12E8. They are located in the crevice between helices $\alpha 4$ and $\alpha 5$, distal to the $\alpha 4$ - $\alpha 5$ loop. No identically equivalent ligands are observed at the interface between the two BAX $\alpha 4$ $\alpha 5$ surfaces but some solvent

or detergent occupies this space, further highlighting the difference in lipid binding between BAX and BAK. Further extraneous electron density, modelled here as diethylene glycol, is observed between the $\alpha 2$ - $\alpha 3$ connection and $\alpha 5$ of both BAK moieties, but again, not of BAX. This 'ligand' can access the hydrophobic space between the two $\alpha 4$ $\alpha 5$ - $\alpha 5'$ $\alpha 4'$ platforms via a narrow opening between BAK $\alpha 5$ (G133) and BAX $\alpha 5$ (V110, F114) although no electron density is visible in this opening.

Type B crystals lysoPC crystals

In crystals grown in the presence of lysoPC, the asymmetric unit contains a single D2 sandwich

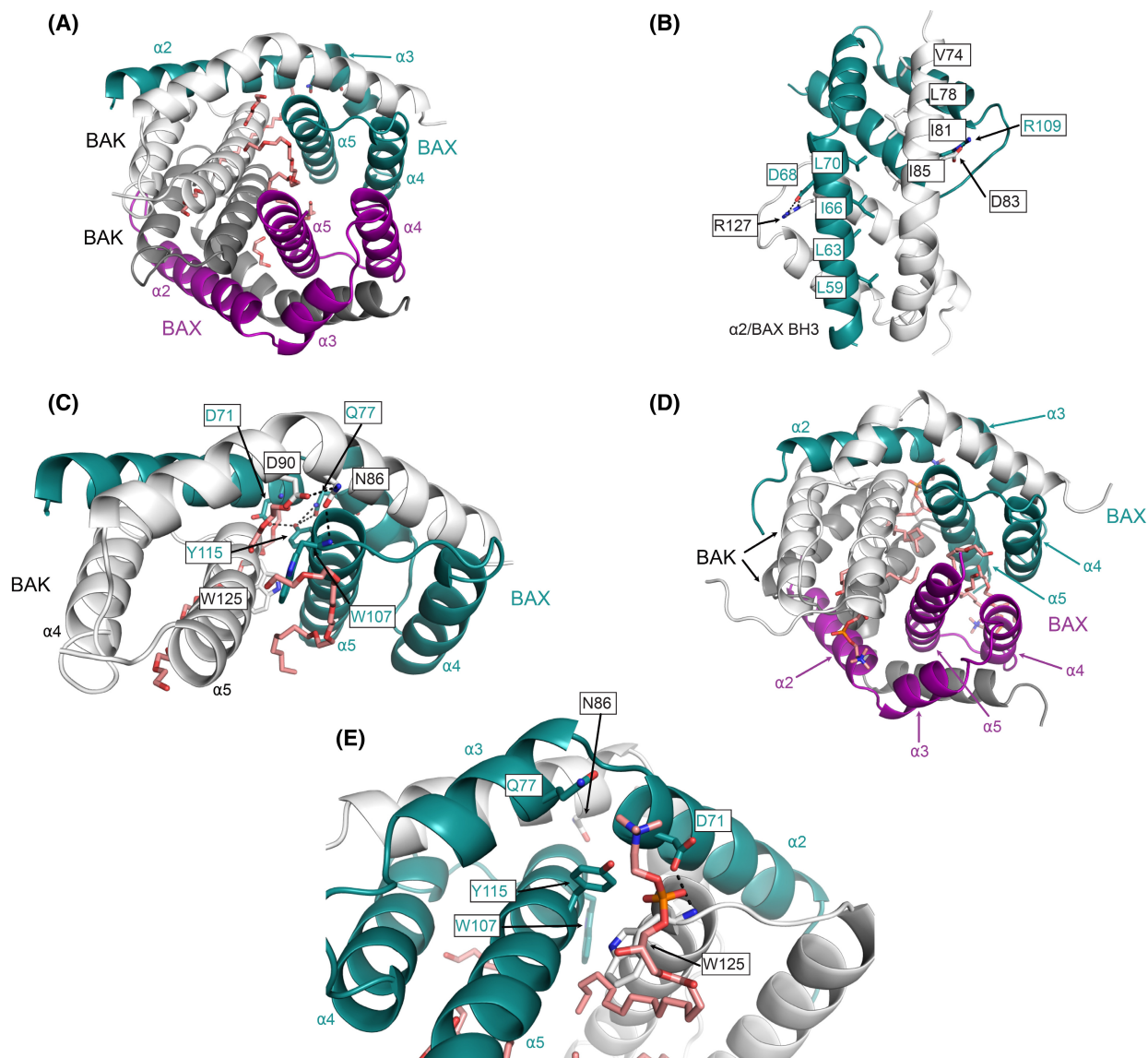


Fig. 5. BAK-BAX heterodimers and lipid binding. (A) Type A crystals of the BAK-BAX heterodimer in the presence of the detergent C12E8. The BAX portion is shown coloured in teal and purple, while the BAK portions are white and grey. The polyethylene glycol (PEG) molecules have been represented as salmon sticks. (B) These structures provide the first picture of BAX BH3 bound in a BAK groove and BAK BH3 bound in a BAX groove. The four signature hydrophobic residues of the BH3 motif for both BAX and BAK are labelled, along with the conserved salt bridge. (C) Close up view of a BAK-BAX heterodimer showing the key lipid binding residues. The PEG-like or detergent molecules are mostly concentrated at the hydrophobic $\alpha4\alpha5-\alpha4'\alpha5'$ platform. BAX W107 does not insert next to BAK G133, but instead a fragment of PEG or detergent fills this space. BAK W125 cannot insert due to the presence of BAX Y115. (D) Type B crystals of the BAK-BAX heterodimer in the presence of the lipid lysoPC. Coloured as per panel a. The lysoPC molecules are shown as salmon sticks. (E) A close up view of the lysoPC binding site in one of the BAK-BAX heterodimers. There are no direct interactions between the protein and the lysoPC molecule. The choline head group is positioned between BAX Q77 and D71, with the phospho head group close to the backbone of BAK W125. The long hydrocarbon tail snakes around the sidechain of BAK W125, which cannot insert due to the presence of BAX Y115.

(Fig. 5D). Similarly to the C12E8 structure, the BAK $\alpha4\alpha5$ platforms face off as do the BAX platforms, however, with different geometry. Unlike the C12E8 structure, clear density for two lipid molecules lies at the heart of the tetramer with their phosphates

at the W125 amide NH of BAK and the cholines near BAX Q77 (Fig. 5E). BAX W107 again does not insert next to BAK G133, but here there is no ligand density. Rather BAK $\alpha3$ collapses into this space (Fig. S9).

Functional role of Y115

The observation of asymmetric BAX core dimers in the presence of lipid and the apparent role of Y115 in that asymmetry led us to investigate a possible functional role for Y115 in BAX-mediated membrane permeabilisation. We were particularly focused on the role of the tyrosyl hydroxyl and its potential to engage phospholipid head groups in the asymmetric conformation. BAX mutants D71N and Y115F, to disrupt the hydrogen-bonding network around Y115 (Fig. 2D), were expressed and purified on a BAX full-length (FL) background, with the cysteines mutated to serines (Fig. S10). Our attempts to also generate Y115A and the Y115F/D71N double mutant were unsuccessful.

The thermal stability of BAX FL D71N was dramatically reduced compared with wild-type FL, BAX FL Y115F less so (Fig. 6A, Fig. S11). We have previously shown with BAK (and for BOK [23,24]) that reduced stability of the monomeric protein results in increased auto-activity, while increased stability is a barrier to activation [25]. The D71N FL mutant correspondingly showed increased activity in the absence of a BH3 stimulus compared with wild-type, both on liposomes and on isolated mouse liver mitochondria (Fig. 6B,C, Fig. S11). The Y115F FL mutant, however, showed low level activity (like wild-type) in the absence of BH3-stimulus, but was consistently less active than wild-type after activation with BIM BH3 peptide or tBID (Fig. 6B,C). Similar results were obtained both on liposomes and isolated mitochondria.

One potential difference for this activity would be capacity to bind lipid, so we performed lipid mass spectrometry on purified hexameric samples of wild-type, D71N and Y115F $\alpha 2$ - $\alpha 5$ core-dimers to compare the relative amount of lipid bound (Fig. 6D, Fig. S12). BAX wild-type pulled down 2342 pmol per μg of protein, which equates to approximately 21 lipid molecules per BAX protomer. BAX D71N hexamers pulled down slightly fewer lipids (75% of WT or 16 molecules per BAX protomer), while Y115F bound just over half (56% or 12 lipid molecules per BAX protomer) of the lipid amount observed in the WT hexamers. This is suggestive of impaired lipid binding capacity in BAX Y115F due to the loss of the hydroxyl group. We additionally solved the structure of BAX D71N dimers from hexamer fractions (Table 1, Fig. S13). The arrangement of molecules in these crystals was similar to that seen for type 4 crystal above, with an asymmetric dimer, consistent with BAX D71N having reduced, but not absent, bound lipid. We were unable to crystallise the BAX Y115F dimers.

Discussion

The BAX core dimer structure revealed in the type 1 crystals is not materially different from the low-resolution structure obtained from crystals of the dimer fused to GFP. The architecture is identical, but the current image affords a high-resolution view. The shape complementarity at the core dimer interface is approximately 0.70 over 1000 \AA^2 of buried surface area on all four copies in the asymmetric unit. The tetrameric assembly within type 1 and type 2 crystals arises from the close packing of opposing $\alpha 4\alpha 5$ - $\alpha 5'\alpha 4'$ surfaces at the heart of the pseudo-D2 symmetric particle. This close packing excludes the possibility of any lipid being trapped between the two hydrophobic surfaces at the heart of the tetramer.

A feature of the core dimer structures of BAK is the frequency with which an anion (often the phosphate moiety of a lipid) is observed bound at the exposed N-terminus of helix $\alpha 5$. Despite the BAX core dimer type 1 crystals growing from concentrated citrate, only water molecules are observed bound at this site in the tetrameric particles. Sequence differences may also play a role here. BAX residue D71 is the structural homologue of BAK N87, and its proximity to the putative anion binding site may compromise the capacity of that site to so function. Another consideration is the proximity of the second dimer in the tetrameric particles of type 1 and type 2 BAX dimer crystals.

X-ray diffraction datasets from two different crystal forms of the hexamer fraction, prepared without either detergent or lipid additions, led to convincing molecular replacement solutions but not to satisfactorily refined structures (discussed in more detail under methods). Both suggested trimeric assemblies of dimers similar to that eventually observed in the type 3 crystals which grew in the presence of lysoPC. The effect of the lysoPC, if any beyond aiding crystallisation, appears to have not involved disassembly of the trimer.

The pseudo-D3 particle observed in the type 3 crystals of the hexamer fraction is reminiscent of a similar structure of trimers of BAK core dimers (Fig. 3A) [17]. In that case, bacterial lipids are observed to mediate interactions between dimers in the hexamer and protein contacts between the dimers are minimal. For BAX, the particle has similar dimensions and could similarly encapsulate bacterial lipids, though structural evidence for that in this case is absent. Like the D3 particle of BAK core dimers, protein-protein interfaces between the BAX core dimers are small ($< 200 \text{\AA}^2$), consistent with the hexamer being a

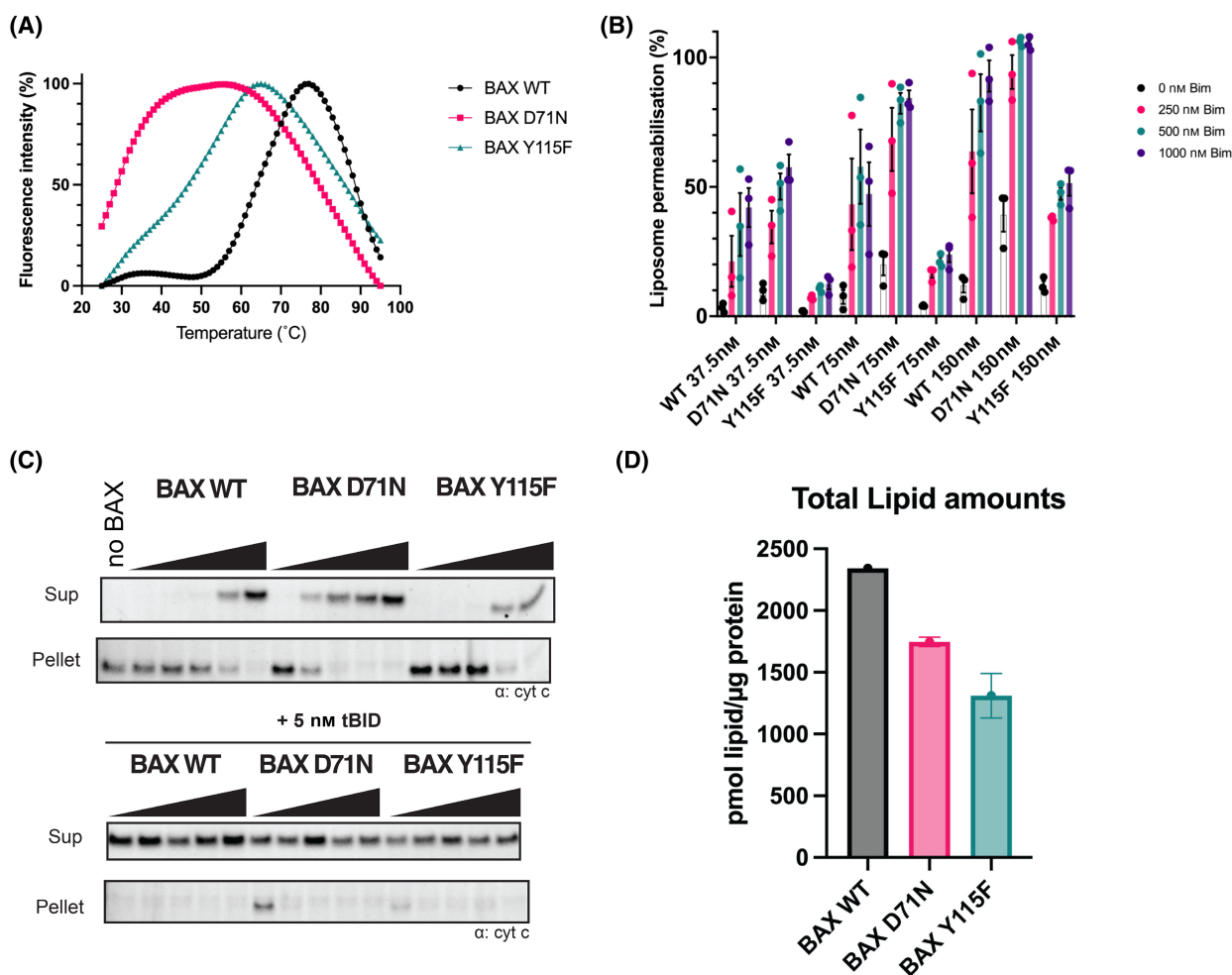


Fig. 6. BAX lipid binding mutants show altered lipid binding and permeabilisation activity. (A) Thermal denaturation curves for full-length BAX wild-type (WT), D71N and Y115F. Five micrometre of BAX WT or mutant was mixed with SYPRO® Orange and the fluorescence signal measured as the protein was heated from 25 to 95 °C. The mean of two technical replicates is plotted. Data shown are the most representative curves for each mutant from three independent experiments. The results from individual experiments are in Fig. S11. (B) Liposome permeabilisation assay with full-length BAX and BAX mutants. Full-length BAX WT or mutant and BIM BH3 were mixed at the specified concentrations and added to 5 μ M of 5(6)-carboxyfluorescein containing liposomes consisting of a mixture of lipids mimicking the mitochondrial outer membrane. The fluorescence signal was background subtracted using a liposome only sample and normalised to dye release from liposomes treated with the detergent CHAPS. Bars represent the mean, with error bars showing SEM, of three independent experiments. Individual independent experimental values (mean of two technical replicates per experiment) are shown as dots. (C) Mouse Liver Mitochondria (MLM) cytochrome *c* release assay. BAX and truncated BID (tBID) were added to isolated mouse liver mitochondria at the specified concentrations and incubated for 1 h at 37 °C. Supernatant and pellet fractions were immunoblotted for cytochrome *c*. All data shown are representative of three independent experiments. Results from repeat experiments are shown in Fig. S11. (D) Assessment of total amount of lipid bound to hexameric fractions of BAX core-dimer mutants by lipid mass spectrometry. Lipid derives from the expression of these constructs in *E. coli*, as previously observed for BAK dimers [17]. Results shown are the mean of two technical replicates, with error bars representing standard deviation.

proteo-lipidic particle wherein the protein has assembled around the lipidic core. However, unlike BAK, the BAX particle does not display preferred binding sites for lipid head groups. In the case of BAK, these led to the sn1 and sn2 acyl chains crosslinking the dimers in the particle. In the case of BAX, the cross-linking appears non-specific.

The type 4 crystal structure illustrates the dependence of the quaternary and/or crystal structure of the BAX core dimers on the lipid environment. Dissolution of the D3 particle in the presence of the short chain lipid is similar to the behaviour of the BAK core dimer D3 particle when it is exposed to detergents and/or short chain lipids. The exposed hydrophobic edges of BAX helix α 4

mediate contacts between dimers in both the D3 assembly and the helical assembly. Small differences in the atomic details of the $\alpha 4$ - $\alpha 4$ contacts underlie the different assemblies, but the small size of the buried protein surfaces again imply that the assembly is largely determined by the lipid.

An unexpected finding from these studies is the presence of asymmetric dimers exclusively in structures that are accompanied by lipid. Even in those cases, a mixture of symmetric and asymmetric dimers is found. The asymmetry is observed adjacent to Y115, the structural counterpart of which is G133 in BAK (Fig. 1). It is marked by the insertion of BAX W107' into the interior of the core dimer (in a manner similar to that observed with BAK W125') with an accompanying exposure of Y115 from the core dimer interior into the $\alpha 4\alpha 5$ - $\alpha 5'\alpha 4'$ surface. The anomalous location of W107' requires displacement of the $\alpha 2$ - $\alpha 3$ linker. Thus, the asymmetry is manifest on both chains of the dimer, on one at W107' and on the other at Y115 and in the pitch of $\alpha 2$. These observations suggest a possible role for Y115 in interactions between BAX core dimers and lipids.

Our results show that either mutation of D71 to asparagine (the BAK homologous residue) or Y115 to phenylalanine destabilises the BAX FL monomer. The destabilisation of the D71N mutation leads to the expected constitutive activation on both liposomes and mitochondria. This mutant also showed slightly lower lipid binding capacity, but the effect of this on the permeabilisation activity appears to be overshadowed by the dramatic loss of monomeric stability. The Y115F mutation also destabilises the monomer, though not as dramatically as D71N. However, rather than constitutive activation, this mutation leads to similar levels of auto-activity to wild-type, and lower capacity for permeabilisation upon BH3-only stimulus. This is likely due to the dramatic reduction in lipid binding capacity (56% of WT levels), consistent with a proposed role for Y115 in lipid binding. Although a lower binding affinity for BH3-only proteins cannot be conclusively ruled out, the Y115 hydroxyl is not directly involved in BH3 binding [18], so this is an unlikely explanation.

In a seminal paper describing the essential role of helices $\alpha 2$ - $\alpha 5$ (core domains) in the membrane-permeabilising properties of BAX [26], various mutants of BAX were characterised. These included the quadruple substitution of residues $^{113}\text{LFYF}^{116}$ with alanine, a mutant that lost its capacity to oligomerise and its membrane activity. Recently, a network analysis [27] has again focussed attention on these residues [28]. Individual alanine replacements at these four residues all destabilise BAX and render it constitutively active on

both liposomes and mitochondria, but certain triple mutants destroy activity by blocking the capacity of BAX to form core dimers [28]. The difference between the constitutively active Y115A mutant and the less active Y115F mutant reported here is noteworthy. The alanine mutation likely results in significantly greater destabilisation than the mutation to phenylalanine. Indeed, we were unable to produce sufficient amounts of the Y115A mutant to conduct our experiments. Perhaps the smaller alanine side-chain allows for more flexibility and for other residues able to contribute to lipid binding, or the level of destabilisation and auto-activation can compensate for lower levels of lipid binding.

Although no convincing evidence emerges for a specific lipid-binding site in these structures of BAX core dimers, non-specific association with lipid is implied by the assembly of core dimers in the crystal types 3 and 4. The dependence of the assembly of core dimers on the lipid environment supports a role for the membrane in the oligomerisation of activated BAX molecules during apoptosis. Unlike BAK where structural evidence supports the linking of dimers via the sn1 and sn2 acyl chains of individual lipids [17] no such evidence is found here for BAX. BAK has been shown to oligomerise faster than BAX [29]. While part of this can be explained by the need for membrane recruitment of BAX, a BAX mutant (S184V) that is constitutively associated with mitochondria still displays slower assembly kinetics. Differences in lipid binding may thus manifest in differences in the kinetics of oligomerisation. Further work is needed to investigate whether this is the case.

Lv *et al.* [16] reported a structure of the BAX core dimer bound to a bicelle. The NMR spectrum of their soluble, core dimer material, constructed identically to ours and presumably the D2 tetramer we describe, showed no signal for residues F114, Y115 and F116. Resonances for these residues appeared in the bicelle-bound BAX core dimer. These studies confirmed the helical organisation of the core dimer but resulted in a structure in which the $\alpha 4\alpha 5\alpha 5'\alpha 4'$ platform is flatter than observed in the D2 soluble assembly or in the symmetric dimers of type 3 and type 4 crystals. In their model that platform is packed against the acyl chains of long-chain lipids exposed by the displacement of the short-chain lipids by the core dimer. In the 15 lowest energy structures reported (PDB: 6L8V), W107 is always projected outwards from the $\alpha 4\alpha 5$ - $\alpha 5'\alpha 4'$ surfaces and never buried in the core dimer interior. Neither is there any evidence in the ensemble of structures in PDB: 6L8V for the anomalous pitch in $\alpha 2$. Thus, the features we describe in asymmetric

dimers, and which are only observed in the presence of lipid, are not features of the BAX core dimer-bicelle complex. The size of the bicelles is carefully controlled to allow only a single core dimer to bind per bicelle. All of the presented structures have limitations as surrogates for understanding what is happening on the surface of the outer mitochondrial membrane, and yield no insight into the role of $\alpha 6$ – $\alpha 9$ in permeabilisation and lipid binding. Despite this, our data suggest that the asymmetric conformations of Y115 and W107 could be involved in the formation of lipid-induced higher order oligomeric structures within the membrane.

The observation of asymmetry in the presence of lipid is intriguing as core dimers are presumed, at least initially, to be symmetric in the outer leaflet of the MOM but are required to transition from that environment to lining the pore. There are opposing models for how dimers line the pore [3], an asymmetric disposition in the pore lumen with one half in the intra membrane space and one half located at the upper leaflet [30] versus a symmetric orientation with dimers evenly distributed across the lumen [31]. In either case, symmetric interactions are in play, either in the transition to a symmetric orientation, or in maintenance of asymmetry in the lumen. Thus, the structures presented here are another snapshot into the possible conformations that BAX can adopt in lipid environments and highlight the complexity of the long standing question as to how lipids are involved first in BAX core dimer formation, and subsequently in the formation of the apoptotic pore.

Materials and methods

Protein production and characterisation

All BAX constructs have their wild-type cysteine residues mutated to serine (C62S, C126S).

The sequence encoding the core domain of BAX ($\alpha 2$ – $\alpha 5$, residues D53–K128) was cloned into the pGEX-6P-3 vector and transformed into BL21 (DE3) *E. coli* cells. Cells were grown at 37 °C and expression was induced by 0.2 mM IPTG and harvested after 2–3 h. GST-fusion proteins were purified using a glutathione column after cell lysis in GST buffer (50 mM Tris pH 8.0, 150 mM NaCl, 1 mM EDTA), and on-column cleavage was performed with PreScission protease. Five residues from the vector (GPLGS) remain at the N-terminus of the construct. The BAX core domain was eluted from the column in GST buffer and purified by anion exchange chromatography, yielding two peaks that were further purified by gel filtration in TBS (20 mM Tris pH 8, 150 mM NaCl) (Superdex S200 Increase 10/300, Cytiva, Marlborough, MA, USA). Two species of MW approximately 40 and 63 kDa, dimers of core dimers

(tetramers) and trimers of core dimers (hexamers) were separately crystallisable. BAX D71N and BAX Y115F core dimers were expressed and purified in the same way.

The core domain of human BAK ($\alpha 2$ – $\alpha 5$, S68–H145) linked via ((GGS)₄G) to human BAX core domain as described above was cloned into pGEX-6P-3 and expressed in *E. coli* BL21 (DE3) cells. Cells were lysed in GST buffer, and the GST-fusion proteins purified as for BAX proteins described above. Further purification by gel filtration (Superdex S75 10/300) in TBS yielded an elution profile consistent with a dimer of the above fusion protein.

Full-length BAX constructs and single mutants were cloned into a pTYB1 vector and expressed in *E. coli* and purified as previously described [5]. Briefly, the cells were lysed in TBS (20 mM Tris pH 8, 150 mM NaCl) and purified firstly by chitin affinity chromatography, followed by size exclusion chromatography (Superdex 75 10/300, Cytiva) in TBS.

Crystallography: BAX Core dimers

Crystallisation experiments were all performed by sitting drop vapour diffusion at 20 °C with drops of 150 : 150 nL unless otherwise specified. X-ray diffraction data were collected at the Australian Synchrotron Beamline MX2 (Tables 1 and 2) and processed with XDS [32].

Two crystal forms were grown from the tetramer fraction, one from protein (6 mg·mL⁻¹) with 1.44 M sodium citrate, 0.01 M TCEP (type 1) and the other from protein (10 mg·mL⁻¹) with 27% PEG MME550, 0.01 M zinc sulfate, 0.1 M NaMes pH 5.6 (type 2). Both were cryoprotected with 10% ethylene glycol. A solution for the type 1 crystals was found by molecular replacement with PHASER [33] using the low-resolution image of the BAX core dimer previously published (PDB: 4BDU) [7]. Chains E: and F: of that structure comprise one core dimer and four copies of this dimer were found arranged as two tetrameric particles with pseudo D2 symmetry. Subsequent model building in COOT [34] and refinement in PHENIX [35] led to the structure described (Table 1). Type 2 crystals have a large asymmetric unit volume. Here the tetrameric particle as determined in the type 1 crystals was used as the initial search object and eventually 9 copies of that tetramer were found and refined (Table 1).

The initial crystals grown from the hexamer fraction contained no detergent or lipid-based additives. Twinned monoclinic crystals grew from protein (13.5 mg·mL⁻¹) with 0.1 M trisodium citrate (pH 3.5), 0.02 M sodium HEPES (pH 6.8), 2 M ammonium sulfate, 0.33% (w/v) of each of 1,3,5 pentanetricarboxylic acid, 5-sulfosalicylic acid and trimesic acid. Tetragonal crystals grew from protein (11.3 mg·mL⁻¹) with citrate buffered 2.3 M ammonium sulfate. Both of these crystal forms gave convincing molecular replacement solutions (final TFZs of 9.1 and 14.6 respectively) based on search objects derived from the core dimers from type 1 crystals, but neither could be satisfactorily refined. Both indicated the presence of a hexameric particle, a trimer of dimers, with pseudo D3

Table 2. Crystallographic data table for BAK-BAX core heterodimer structures. Statistics for the highest-resolution shell are shown in parentheses.

	Type A. C12E8 crystals 8SRV	Type B. lysoPC crystals 8SRX
Space group	P6 ₁	C2 ₁
Unit cell		
<i>a</i> , <i>b</i> , <i>c</i> (Å)	43.96, 43.96, 220.04	158.17, 45.56, 43.71
α , β , γ (°)	90, 90, 120	90, 101.76, 90
Wavelength (Å)	0.9537	0.9537
Resolution range (Å)	38.07–2.39 (2.48–2.39)	38.71–2.09 (2.17–2.09)
Total reflections	178 297 (17 721)	113 430 (11 090)
Unique reflections	9406 (939)	18 141 (1776)
Multiplicity	19.0 (18.9)	6.3 (6.2)
Completeness (%)	99.9 (99.9)	99.7 (98.2)
// $\sigma(I)$	20.2 (1.6)	8.6 (1.3)
<i>R</i> _{merge}	0.143 (2.05)	0.199 (1.42)
CC 1/2	0.99 (0.53)	0.99 (0.41)
<i>R</i> -work	0.2132 (0.2977)	0.2161 (0.3201)
<i>R</i> -free	0.2471 (0.3661)	0.2654 (0.3823)
Number of non-hydrogen atoms	2537	2708
Macromolecules	2455	2469
Ligands	81	125
Solvent	1	114
RMS		
Bonds (Å)	0.005	0.006
Angles (°)	1.02	1.05
Ramachandran		
Favoured (%)	96.07	94.10
Outliers (%)	1.31	2.30
Average B-factor		
Macromolecules	62.98	36.41
Ligands	61.49	46.01
Solvent	84.69	40.66

symmetry encompassing a void large enough to contain bacterial lipids though none could be visualised. Contacts between the core dimers around the three-fold axis in both of these assemblies involved pairs of $\alpha 4$ helices.

An interpretable crystal form from the hexamer fraction was obtained after first incubating hexamer at 9.9 mg·mL⁻¹ with 5 mM 2-stearoyl-*sn*-glycero-3-phosphocholine (LysoPC). Crystals grew from 1.4 M trisodium citrate, 0.1 M Hepes, pH 7.5. These crystals, type 3, were solved by molecular replacement using a search object derived from the type 1 crystals. Four copies of one half of a core dimer ($\alpha 2$ of one polypeptide in the $\alpha 3\alpha 4\alpha 5$ groove of the partner) were located by molecular replacement and a near-complete model for the hexamer resulted from successive rounds of model building and refinement. Pairs of $\alpha 4$ helices mediate contacts between the core dimers in the pseudo D3-symmetric particle.

Type 4 crystals grew from the hexamer fraction at 7.5 mg·mL⁻¹ in the presence of 5 mM di-octanoyl phosphatidylserine (~ 5-fold molar excess over the core domain

construct), 2.25 M ammonium sulfate, 9% v/v DL maleate-MES-tris pH 7, 0.1 M trisodium citrate (frozen in 25% glycerol). Two copies of the core dimer as determined from the type 1 crystals were located by molecular replacement with PHASER [33]. They are arranged side-by-side via contacts between $\alpha 4$ residues.

Assessment of buried surface area was performed using SC [36].

All structure figures were generated with PYMOL v2.5.5 (Schrodinger, Inc., New York, NY, USA).

Crystallography: BAK-BAX Hetero-core dimers

Diffraction-quality crystals were only obtained in the presence of detergent or lipid. Type A crystals grow from protein (6 mg·mL⁻¹) with 30% PEG MME 2000, 100 mM potassium thiocyanate and 0.01% C12E8 at 8 °C. A search model was constructed from the $\alpha 2$ -helix of the BAX core-domain dimer (PDB: 4BDU) [7] with $\alpha 4$ - $\alpha 5$ of BAK in its core-domain dimer (PDB: 4U2U) [8]. Four copies of this object were found with PHASER and subjected to rounds of building in COOT and refinement in PHENIX to complete the model. Type B crystals grow from protein (6 mg·mL⁻¹), 100 mM bis-Tris chloride pH 5.5, 25% PEG 3350, 200 mM sodium acetate, 10 mM LysoPC at 8 °C. Four copies of a search object like that described above but taken from the type A crystal structure were located with PHASER [33] and refined with COOT [34] and PHENIX [35] (Table 2).

Crystallography: D71N BAX Core-dimer

Crystals were grown from drops with 100 nL protein (10 mg·mL⁻¹) and 100 nL 0.2 M sodium citrate tribasic dihydrate, 20% PEG3350 at 18 °C. Four copies of a type 4 WT dimer were found with PHASER [33] and subjected to rounds of building in COOT [34] and refinement in PHENIX [35] to complete the model (Table 1).

Thin layer chromatography (TLC)

Concentrated samples of the BAX core domain tetramer or hexamer were slowly pipetted onto marked spots near the base of aluminium-backed, silica gel 60 TLC plates. Plates were placed in glass jars containing chloroform/methanol/water [25 : 10 : 1 (v/v/v)] to a level below where samples were loaded. Samples were run until the solvent front was close to the top of the TLC plate, and plates were dried. Dried plates were stained with ninhydrin or phosphomolybdic acid, then dried and heated with a heat gun to reveal stained lipid species.

Thermal shift assay

5 μ M of full-length BAX in TBS was mixed with SYPRO® Orange (1 : 550 dilution, Sigma, Saint Louis, MO, USA) and a temperature gradient of 1°/50 s from 25 to 95 °C

applied to the samples. The fluorescence signal was measured at every degree using the FRET channel of a C1000 thermocycler equipped with a CFX384 Real-Time System fluorescence reader (Biorad, Hercules, CA, USA). All experiments were performed in duplicate at least three times.

Liposome assay

Liposomes containing a mixture of lipids mimicking the mitochondrial outer membrane were prepared as previously described [7,37]. All lipids were purchased from Avanti Polar Lipids (Alabaster, AL, USA). Liposomes were made with a mole percent mixture of 46% 1-palmitoyl-2-oleoyl-sn-glycero-3-phosphocholine (POPC), 25% 1,2-dioleoyl-sn-glycero-3-phosphoethanolamine (PE), 11% L- α -phosphatidylinositol from bovine liver (PI) 10% 1,2-dioleoyl-sn-glycero-3-phospho-L-serine, 8% 1',3'-bis[1,2-dioleoyl-sn-glycero-3-phospho]-sn-glycerol (cardiolipin). Chloroform solutions of the lipids were mixed in the described ratio and dried under a stream of nitrogen. The lipid film was resuspended in 50 mM 5(6)-carboxyfluorescein. Resuspended lipids were frozen and thawed several times and then extruded an odd number of times (more than 20) through a membrane with a pore size of 100 nm and stored at 4 °C. Excess dye was removed from the liposomes using a PD10 column immediately before use.

Human BIM BH3 peptide (Ac-DMRPEIWIQAQLR-RIGDEFNAYYARR-NH₂) was purchased from Mimotopes (Melbourne, Vic, Australia) and stored as a 10 mM stock in DMSO. BAX and BIM BH3 were diluted to the concentrations specified in SUV buffer and added to liposomes with 5 μ M lipid in a final reaction volume of 150 μ L in Falcon 96-well U-bottom tissue culture plates (Corning Costar, Cambridge, MA, USA). Fluorescence (excitation at 485 nm, emission at 535 nm) was measured every 2 min in a Chameleon V plate reader (LabLogic Systems, Sheffield, UK) over the course of 1 h. Experiments were performed with two technical replicates at least three times. The fluorescence signal was background subtracted using a liposome only sample and normalised to dye release from liposomes treated with the detergent CHAPS.

Mitochondrial assays

Mouse liver mitochondria (MLM) were isolated from male *Bak*^{-/-} *C57BL/6* mice (ranging 150–155 days old) [38] that were bred and maintained at the Walter and Eliza Hall Institute of Medical Research Animal Facility. All animal experiments were approved by the WEHI Animal Ethics Committee (WEHI internal ethics number 2022.014) and were conducted in accordance with the Prevention of Cruelty to Animals Act (1986) and the Australian National Health and Medical Research Council Code of Practice for the Care and the Use of Animals for Scientific Purposes (1997). Euthanasia of adult mice by cervical dislocation was performed by trained Bioservices staff followed by

harvesting of mouse livers. Individual barrier cages were used for permanent housing in all areas (e.g. Individually Ventilated Cages or Exhaust Ventilated Cages). Mice were kept in open topped cages for short periods. Rooms were controlled at appropriate temperature and humidity levels. Cages contained suitable bedding material (e.g. Corn cob, Puracell) and environmental enrichment for shelter, nesting and foraging activities (e.g. plastic domes, tissues, mash, sunflower seeds). Food and water were provided *ad libitum*. Single housing of mice was minimised and a maximum of 6 adult mice were housed per cage.

Isolation was conducted as described previously [39]. Isolated MLMs were diluted to 1 mg·mL⁻¹ in MELB (100 mM KCl, 2.5 mM MgCl₂, 100 mM sucrose, 20 mM HEPES/KOH pH 7.5) and supplemented with complete EDTA-free protease inhibitor cocktail (Roche, Mannheim, Germany) and 4 mg·mL⁻¹ pepstatin A (Sigma Aldrich). Isolated MLMs were incubated with BAX and cBID at the concentrations specified and incubated at 37 °C for 1 h. Samples were spun at 10 000 *g* at 4 °C for 10 min and the supernatant and pellet fractions immunoblotted for cytochrome *c*.

cBID was expressed and purified as described previously [40,41]. The construct was expressed as a GST fusion using the pGEXT4T-1 vector in BL21 (DE3) *E. coli* cells. Bacterial cells were cultured at 37 °C in super broth until an optical density of 0.6 was achieved at 600 nm, cells were then induced for 16 h with 1 mM isopropyl β -D-1-thiogalactopyranoside at 18 °C. The resultant cells were harvested by centrifugation and lysed using a French press in a lysis buffer consisting 50 mM Tris pH 8, 1 mM EDTA, 150 mM NaCl and 1.5 mg·mL⁻¹ DNase I. The cBID GST-fusion protein was purified using glutathione resin (GenScript, Piscataway, NJ, USA). The GST fusion was removed by proteolysis using thrombin protease (1 unit, Sigma, cat# 10602400001) and adding CaCl₂ to a final concentration of 1 mM, incubating overnight at 4 °C and eluting cBID as the flow through from the column.

SDS/PAGE and western blotting

Samples were resolved by SDS/PAGE (Bolt™ 4–12% Bis-Tris gels, Invitrogen, Waltham, MA, USA) and transferred to 0.22 μ m nitrocellulose membranes. Membranes were blotted with anti-cytochrome *c* (1 : 2000, #556433, BD Biosciences, Franklin Lakes, NJ, USA) and detected with IRDye® 800CW goat anti-mouse IgG secondary antibody (1 : 20 000, P/N 926-32210, Licor Biosciences, Lincoln, NE, USA). Immunoblotted membranes were imaged on a ChemiDoc™ MP Imaging System (Bio-Rad).

Lipid identification and quantification

Lipids were extracted from purified WT BAX α 2- α 5, Y115F BAX α 2- α 5 and D71N BAX α 2- α 5 protein using a

monophasic lipid extraction protocol, similar to that previously described [17,42]. Dried protein pellets were resuspended in 100 μL 60% aqueous methanol. For each 10 μg protein, 1 μL chloroform containing lipid standard PE (33 : 1) d7, PG (33 : 1) d7 and CL (56 : 0) was added. An additional 208 μL methanol, 133 μL chloroform and 59 μL milli-Q water were then added to each sample to achieve a final extraction ratio of 0.74 : 1 : 2 methanol:chloroform:water. Samples were then incubated at room temperature on ThermoMix at 1000 rpm for 30 min, followed by centrifugation at 21,000 g for 15 min. Supernatants were collected and transferred to new Eppendorf tubes and dried in a SpeedyVap vacuum evaporator. Dried lipid extracts were then reconstituted into 200 μL of a 2-propanol: methanol: chloroform mixture (4/2/1, v/v/v) and transferred to glass vials then stored at -80°C prior to further analysis. Lipid analysis was performed as previously described, with some modification [43]. Lipid extract was diluted in 2-propanol: methanol: chloroform mixture (4/2/1, v/v/v) containing 20 mM ammonium formate, then introduced into an Orbitrap Fusion Lumos Mass Spectrometer (Thermo Scientific, Waltham, MA, USA) using a Triversa Nanomate nESI source (Advion, Ithaca, NY, USA), operating with a spray voltage of 1.1 kV and a gas pressure of 0.3 psi. The mass spectrometer transfer tube was set at 150°C and the RF lens set to 10%, with a AGC target of 50%. Mass spectra were collected over a mass range of 350–1600 m/z with a mass resolving power of 500 000 for 3 min in negative ionisation mode. A Field Asymmetric Ion Mobility Spectrometry (FAIMS) interface (FAIMS Pro, Thermo Fisher Scientific, San Jose, CA, USA) was interfaced with the mass spectrometer for selective enrichment and analysis of cardiolipin (CL). Lipid extracts were reconstituted in 2-propanol: methanol: chloroform mixture (4/2/1, v/v/v) and introduced to the mass spectrometer, using a FAIMS compensation voltage of 61 V in negative ionisation mode (optimised for the cardiolipin $[\text{M}-2\text{H}]^{2-}$ precursor ion charge states) [44,45]. Mass spectra were collected using an RF lens setting of 20% and an AGC target setting of 100% for 3 min, with a mass resolving power of 500 000. Data analysis of the resultant mass spectra was carried out using LIPIDSEARCH 5.0 software (Thermo Scientific and Mitsui Knowledge Industry) with automated peak picking, correction of ^{13}C isotope abundances and identification of lipids at the 'sum composition' level of annotation using an in-house generated lipid database, as described previously [45]. For peak picking, precursor ion intensity threshold was set at 3 times the observed noise intensity with the mass tolerance set at 3.0 ppm. For lipid ion identification and quantification, the isotope threshold was 0.1% and the max isotope number was set at 1. LipidSearch outputs were further processed with in-house developed R scripts, in which the concentration of endogenous lipids were calculated based on the peak area ratio of individual lipids compared to their corresponding internal lipid standards.

Acknowledgements

We thank Richard Birkinshaw for helpful discussions and suggestions. Research in the authors' laboratories was supported by NHMRC project grants (1079706), program grant (1113133), Ideas grant (2001406), fellowships (1116934 PMC, 2009062 PEC), infrastructure support (IRISS 9000719), the Leukaemia and Lymphoma Society (SCOR 7015-18), and the Victorian Government Operational Infrastructure Support scheme. This research was undertaken in part using the MX beamlines at the Australian Synchrotron, part of ANSTO, and made use of the Australian Cancer Research Foundation (ACRF) detector. We also thank C3 crystallisation facility, the Monash Macromolecular Crystallisation Centre and the Bio21-WEHI crystallisation facility for assistance with protein crystallisation. Open access publishing facilitated by The University of Melbourne, as part of the Wiley - The University of Melbourne agreement via the Council of Australian University Librarians.

Conflict of interest

The authors declare no conflict of interest.

Author contributions

MSM, ADC, JMB, STS, LP, AZW, RTU, CL, MJR, SS, ZT planned and performed experiments. MSM, ADC, JMB, GER, PEC, PMC analysed data. PMC, PEC and MSM wrote the manuscript. All authors edited the manuscript.

Data availability statement

The structural data that support these findings are openly available in the wwPDB at BAX Type 1 tetramer (<https://doi.org/10.2210/pdb8G1T/pdb>), BAX Type 2 tetramer (<https://doi.org/10.2210/pdb8SPE/pdb>), BAX Type 3 hexamer (<https://doi.org/10.2210/pdb8SPF/pdb>), BAX Type 4 hexamer (<https://doi.org/10.2210/pdb8SPZ/pdb>), BAX D71N (<https://doi.org/10.2210/pdb8SVK/pdb>), BAK-BAX heterodimer C12E8 crystals Type A (<https://doi.org/10.2210/pdb8SRY/pdb>), BAK-BAX heterodimer lysoPC crystals Type B (<https://doi.org/10.2210/pdb8SRX/pdb>).

References

- 1 Czabotar PE, Lessene G, Strasser A & Adams JM (2014) Control of apoptosis by the BCL-2 protein family: implications for physiology and therapy. *Nat Rev Mol Cell Biol* **15**, 49–63.

- 2 Kvsanakul M & Hinds MG (2015) The Bcl-2 family: structures, interactions and targets for drug discovery. *Apoptosis* **20**, 136–150.
- 3 Czabotar PE & Garcia-Saez AJ (2023) Mechanisms of BCL-2 family proteins in mitochondrial apoptosis. *Nat Rev Mol Cell Biol* **24**, 732–748.
- 4 Robin AY, Iyer S, Birkinshaw RW, Sandow J, Wardak A, Luo CS, Shi M, Webb AI, Czabotar PE, Kluck RM *et al.* (2018) Ensemble properties of Bax determine its function. *Structure* **26**, 1346–1359.e5.
- 5 Suzuki M, Youle RJ & Tjandra N (2000) Structure of Bax: coregulation of dimer formation and intracellular localization. *Cell* **103**, 645–654.
- 6 Moldoveanu T, Liu Q, Tocilj A, Watson M, Shore G & Gehring K (2006) The X-ray structure of a BAK homodimer reveals an inhibitory zinc binding site. *Mol Cell* **24**, 677–688.
- 7 Czabotar PE, Westphal D, Dewson G, Ma S, Hockings C, Fairlie WD, Lee EF, Yao S, Robin AY, Smith BJ *et al.* (2013) Bax crystal structures reveal how BH3 domains activate Bax and nucleate its oligomerization to induce apoptosis. *Cell* **152**, 519–531.
- 8 Brouwer JM, Westphal D, Dewson G, Robin AY, Uren RT, Bartolo R, Thompson GV, Colman PM, Kluck RM & Czabotar PE (2014) Bak Core and latch domains separate during activation, and freed Core domains form symmetric homodimers. *Mol Cell* **55**, 938–946.
- 9 Alsop AE, Fennell SC, Bartolo RC, Tan IK, Dewson G & Kluck RM (2015) Dissociation of Bak alpha1 helix from the core and latch domains is required for apoptosis. *Nat Commun* **6**, 6841.
- 10 Hsu YT & Youle RJ (1997) Nonionic detergents induce dimerization among members of the Bcl-2 family. *J Biol Chem* **272**, 13829–13834.
- 11 Lovell JF, Billen LP, Bindner S, Shamas-Din A, Fradin C, Leber B & Andrews DW (2008) Membrane binding by tBid initiates an ordered series of events culminating in membrane permeabilization by Bax. *Cell* **135**, 1074–1084.
- 12 Birkinshaw RW, Iyer S, Lio D, Luo CS, Brouwer JM, Miller MS, Robin AY, Uren RT, Dewson G, Kluck RM *et al.* (2021) Structure of detergent-activated BAK dimers derived from the inert monomer. *Mol Cell* **81**, 2123–2134.e5.
- 13 Korsmeyer SJ, Wei MC, Saito M, Weiler S, Oh KJ & Schlesinger PH (2000) Pro-apoptotic cascade activates BID, which oligomerizes BAK or BAX into pores that result in the release of cytochrome c. *Cell Death Differ* **7**, 1166–1173.
- 14 Bleicken S, Assafa TE, Stegmüller C, Wittig A, Garcia-Saez AJ & Bordignon E (2018) Topology of active, membrane-embedded Bax in the context of a toroidal pore. *Cell Death Differ* **25**, 1717–1731.
- 15 Uren RT, O'Hely M, Iyer S, Bartolo R, Shi MX, Brouwer JM, Alsop AE, Dewson G & Kluck RM (2017) Disordered clusters of Bak dimers rupture mitochondria during apoptosis. *Elife* **6**, e19944.
- 16 Lv F, Qi F, Zhang Z, Wen M, Kale J, Piai A, Du L, Wang S, Zhou L, Yang Y *et al.* (2021) An amphipathic Bax core dimer forms part of the apoptotic pore wall in the mitochondrial membrane. *EMBO J* **40**, e106438.
- 17 Cowan AD, Smith NA, Sandow JJ, Kapp EA, Rustam YH, Murphy JM, Brouwer JM, Bernardini JP, Roy MJ, Wardak AZ *et al.* (2020) BAK core dimers bind lipids and can be bridged by them. *Nat Struct Mol Biol* **27**, 1024–1031.
- 18 Robin AY, Krishna Kumar K, Westphal D, Wardak AZ, Thompson GV, Dewson G, Colman PM & Czabotar PE (2015) Crystal structure of Bax bound to the BH3 peptide of Bim identifies important contacts for interaction. *Cell Death Dis* **6**, e1809.
- 19 Czabotar PE, Lee EF, Thompson GV, Wardak AZ, Fairlie WD & Colman PM (2011) Mutation to Bax beyond the BH3 domain disrupts interactions with pro-survival proteins and promotes apoptosis. *J Biol Chem* **286**, 7123–7131.
- 20 Ku B, Liang C, Jung JU & Oh BH (2011) Evidence that inhibition of BAX activation by BCL-2 involves its tight and preferential interaction with the BH3 domain of BAX. *Cell Res* **21**, 627–641.
- 21 Burnley BT, Afonine PV, Adams PD & Gros P (2012) Modelling dynamics in protein crystal structures by ensemble refinement. *Elife* **1**, e00311.
- 22 Dewson G, Ma S, Frederick P, Hockings C, Tan I, Kratina T & Kluck RM (2012) Bax dimerizes via a symmetric BH3:groove interface during apoptosis. *Cell Death Differ* **19**, 661–670.
- 23 Ke FFS, Vanyai HK, Cowan AD, Delbridge ARD, Whitehead L, Grabow S, Czabotar PE, Voss AK & Strasser A (2018) Embryogenesis and adult life in the absence of intrinsic apoptosis effectors BAX, BAK, and BOK. *Cell* **173**, 1217–1230.e17.
- 24 Zheng JH, Grace CR, Guibao CD, McNamara DE, Llambi F, Wang Y, Chen T & Moldoveanu T (2018) Intrinsic instability of BOK enables membrane permeabilization in apoptosis. *Cell Rep* **15**, 2083–2094.e6.
- 25 Robin AY, Miller MS, Iyer S, Shi MX, Wardak AZ, Lio D, Smith NA, Smith BJ, Birkinshaw RW, Czabotar PE *et al.* (2022) Structure of the BAK-activating antibody 7D10 bound to BAK reveals an unexpected role for the $\alpha 1$ - $\alpha 2$ loop in BAK activation. *Cell Death Differ* **29**, 1757–1768.
- 26 George NM, Evans JJ & Luo X (2007) A three-helix homo-oligomerization domain containing BH3 and BH1 is responsible for the apoptotic activity of Bax. *Genes Dev* **21**, 1937–1948.
- 27 Chakrabarty B & Parekh N (2016) NAPS: network analysis of protein structures. *Nucleic Acids Res* **44**, W375–W382.
- 28 Bloch NB, Wales TE, Prew MS, Levy HR, Engen JR & Walensky LD (2021) The conformational stability of pro-apoptotic BAX is dictated by discrete residues of the protein core. *Nat Commun* **12**, 4932.

- 29 Cosentino K, Hertlein V, Jenner A, Dellmann T, Gojkovic M, Peña-Blanco A, Dadsena S, Wajngarten N, Danial JSH, Thevathasan JV *et al.* (2022) The interplay between BAX and BAK tunes apoptotic pore growth to control mitochondrial-DNA-mediated inflammation. *Mol Cell* **82**, 933–949.
- 30 Mandal T, Shin S, Aluvila S, Chen HC, Grieve C, Choe JY, Cheng EH, Hustedt EJ & Oh KJ (2016) Assembly of Bak homodimers into higher order homooligomers in the mitochondrial apoptotic pore. *Sci Rep* **6**, 30763.
- 31 Bleicken S, Jeschke G, Stegmüller C, Salvador-Gallego R, Garcia-Saez AJ & Bordignon E (2014) Structural model of active Bax at the membrane. *Mol Cell* **56**, 496–505.
- 32 Kabsch W (2010) Integration, scaling, space-group assignment and post-refinement. *Acta Crystallogr D Biol Crystallogr* **66**, 133–144.
- 33 McCoy AJ, Grosse-Kunstleve RW, Adams PD, Winn MD, Storoni LC & Read RJ (2007) Phaser crystallographic software. *J Appl Cryst* **40**, 658–674.
- 34 Emsley P & Cowtan K (2004) Coot: model-building tools for molecular graphics. *Acta Crystallogr D Biol Crystallogr* **60**, 2126–2132.
- 35 Adams PD, Afonine PV, Bunkoczi G, Chen VB, Davis IW, Echols N, Headd JJ, Hung LW, Kapral GJ, Grosse-Kunstleve RW *et al.* (2010) PHENIX: a comprehensive python-based system for macromolecular structure solution. *Acta Crystallogr D Biol Crystallogr* **66**, 213–221.
- 36 Lawrence MC & Colman PM (1993) Shape complementarity at protein-protein interfaces. *J Mol Biol* **234**, 946–950.
- 37 Kuwana T, Mackey MR, Perkins G, Ellisman MH, Latterich M, Schneider R, Green DR & Newmeyer DD (2002) Bid, Bax, and lipids cooperate to form supramolecular openings in the outer mitochondrial membrane. *Cell* **111**, 331–342.
- 38 Lindsten T, Ross AJ, King A, Zong WX, Rathmell JC, Shiels HA, Ulrich E, Waymire KG, Mahar P, Frauwirth K *et al.* (2000) The combined functions of proapoptotic Bcl-2 family members bak and bax are essential for normal development of multiple tissues. *Mol Cell* **6**, 1389–1399.
- 39 Uren RT, Dewson G, Bonzon C, Lithgow T, Newmeyer DD & Kluck RM (2005) Mitochondrial release of pro-apoptotic proteins: electrostatic interactions can hold cytochrome c but not Smac/DIABLO to mitochondrial membranes. *J Biol Chem* **280**, 2266–2274.
- 40 Brouwer JM, Lan P, Cowan AD, Bernardini JP, Birkinshaw RW, van Delft MF, Sleebs BE, Robin AY, Wardak A, Tan IK *et al.* (2017) Conversion of Bim-BH3 from activator to inhibitor of Bak through structure-based design. *Mol Cell* **68**, 659–672.e9.
- 41 Kluck RM, Esposti MD, Perkins G, Renken C, Kuwana T, Bossy-Wetzell E, Goldberg M, Allen T, Barber MJ, Green DR *et al.* (1999) The pro-apoptotic proteins, bid and Bax, cause a limited permeabilisation of the mitochondrial outer membrane that is enhanced by cytosol. *J Cell Biol* **147**, 809–822.
- 42 Lydic TA, Busik JV & Reid GE (2014) A monophasic extraction strategy for the simultaneous lipidome analysis of polar and nonpolar retina lipids. *J Lipid Res* **55**, 1797–1809.
- 43 Lydic TA, Townsend S, Adda CG, Collins C, Mathivanan S & Reid GE (2015) Rapid and comprehensive ‘shotgun’ lipidome profiling of colorectal cancer cell derived exosomes. *Methods* **87**, 83–95.
- 44 Lee RG, Gao J, Siira SJ, Shearwood A, Ermer JA, Hofferek V, Mathews JC, Zheng M, Reid GE, Rackham O *et al.* (2020) Cardiolipin is required for membrane docking of mitochondrial ribosomes and protein synthesis. *J Cell Sci* **133**, jcs240374.
- 45 Kralj T, Nuske M, Hofferek V, Sani M, Lee T, Separovic F, Aguilar M & Reid GE (2022) Multi-Omic analysis to characterize metabolic adaptation of the *E. coli* lipidome in response to environmental stress. *Metabolites* **12**, 171.

Supporting information

Additional supporting information may be found online in the Supporting Information section at the end of the article.

Fig. S1. Size exclusion trace of BAX wild-type (WT) and mutant tetramer and hexamer fractions.

Fig. S2. Differences between the four dimer copies in the asymmetric unit of the Type 1 crystals.

Fig. S3. Type 2 crystals provide 36 independent images of the core domain in 18 dimers (9 D2-symmetric tetramers) and illustrate a softness in the structure of the $\alpha 2\alpha 3$ layer.

Fig. S4. Alignment of the six BH3-in-groove entities from the type 3 crystals.

Fig. S5. Dimer interfaces between $\alpha 4$ helices in type 3 crystals.

Fig. S6. Thin layer chromatography of BAX($\alpha 2-5$) tetramer and hexamer samples.

Fig. S7. Electron density around sulfate ion.

Fig. S8. Binding of the ‘h0’ residue in the BAK-BAX heterodimers.

Fig. S9. BAX W107 does not insert in the BAK-BAX heterodimer structures.

Fig. S10. Size exclusion trace of BAX full length and mutants.

Fig. S11. Data for repeat experiments in Fig. 6.

Fig. S12. Lipidomic analysis of purified hexameric fractions of BAX core dimers.

Fig. S13. BAX D71N core dimer crystal structure.